Contents

S1 Influence of the Sigmoid parameter d

To test the influence of the parameter d on the critical supersaturation we calculated Köhler curves with Eq. 1. We assumed the particle to consist entirely of an organic (surface-active) substance, i.e., it contains no inorganic co-solute. We further assumed solution ideality, i.e., $a_w = x_w$, where x_w is the mole fraction of water and the organic substance is assumed not to dissociate. The surface tension σ in the Kelvin equation (exponential function in Eq. 1) is calculated as a function of the total composition of the particle using the Sigmoid model (Eq. 2). As such, no bulk depletion is considered. The temperature is set to $T = 25\,°\mathrm{C}$ and the molar volume of water to $v_i N_A = 18.05\,\mathrm{cm}^3\,\mathrm{mol}^{-1}$. In Fig. S1, the results are shown for three different substances, i.e., propionic acid, SDS, and oleic acid, which are covering a broad range of p values. The values for p, σ_i, and $v_i N_A$ which were used for each substance are annotated in the respective panel. The curves with $d = 1$ are highlighted by a thicker, black line because the Eberhart model is a simplified version of the Sigmoid model with $d = 1$.
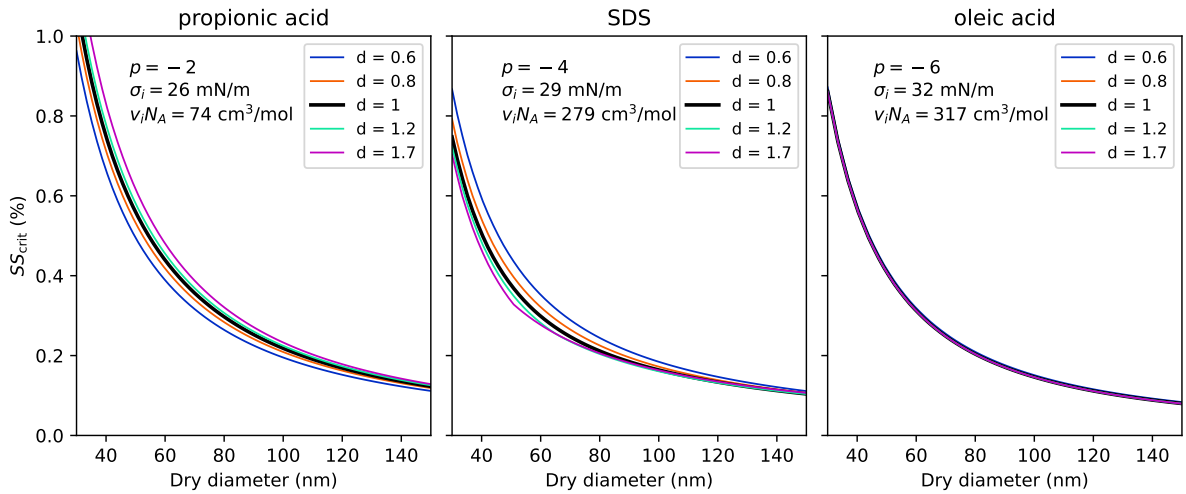

Figure S1: Influence of the Sigmoid model's parameter d: Critical supersaturation as a function of the dry diameter for three different substances and 5 different values for d.

It can be seen that the curves for the various d values are close to each other and in the case of oleic acid overlap entirely. The strongest influence of d on SS_{crit} is observed for the case with SDS. According to the fits with the Sigmoid model in El Haber et al. (2024), $d = 1.65$ for SDS and small dry diameters. For dry diameters between $30\,\mathrm{nm}$ and $60\,\mathrm{nm}$, assuming $d = 1$ leads to an error in $\Delta SS_{\mathrm{crit}}$ of $\approx 0.05\,\%$. This error can be regarded as the maximum overall error, since here we assumed particles consisting entirely of the surfactant and bulk depletion is not considered, both of which enhance the surface tension lowering effect on SS_{crit}. This small maximum error justifies the assumption of $d = 1$ in the Eberhart model for the purpose of calculating SS_{crit}.

S2 Computational flowchart for the quaternary Eberhart –Monolayer model

Set values for
$D_{\text{wet}}, w_{\text{org}}, w_{\text{glu}}/w_{\text{org}}$

Total volume and molecule number
$V = (\pi/6)D_{\text{wet}}^3, \quad n_i^{\text{tot}} = f(V, v_i)$

Guess
$x_2^{\text{bulk}}, x_3^{\text{bulk}}, x_4^{\text{bulk}}$

$x_1^{\text{bulk}} = 1 - x_2^{\text{bulk}} - x_3^{\text{bulk}} - x_4^{\text{bulk}}$

Pseudo-binary water (1)–salt (4) mixture:

Redefined mole fraction: $\psi_4^{\text{bulk}} = \dfrac{x_4^{\text{bulk}}}{x_1^{\text{bulk}} + x_4^{\text{bulk}}}$

Binary Eberhart model: $\sigma_{14} = f^{EB}\left(1 - \psi_4^{\text{bulk}}, \psi_4^{\text{bulk}}\right)$

Surface composition: $\psi_4^{\text{surf}} = \dfrac{v_1(\sigma_1 - \sigma_{14})}{v_1(\sigma_1 - \sigma_{14}) + v_4(\sigma_{14} - \sigma_4)}$

Molecular volume: $v_{14} = v_1\left(1 - \psi_4^{\text{surf}}\right) + v_4\psi_4^{\text{surf}}$

Pseudo-binary salt–water (14)–glucose (3) mixture:

Redefined mole fraction: $\chi_3^{\text{bulk}} = \dfrac{x_3^{\text{bulk}}}{x_1^{\text{bulk}} + x_3^{\text{bulk}} + x_4^{\text{bulk}}}$, etc.

Ternary Eberhart model: $\sigma_{134} = f^{EB}\left(\chi_1^{\text{bulk}}, \chi_3^{\text{bulk}}, \chi_4^{\text{bulk}}\right)$

Surface composition: $\chi_3^{\text{surf}} = \dfrac{v_{14}(\sigma_{14} - \sigma_{134})}{v_{14}(\sigma_{14} - \sigma_{134}) + v_3(\sigma_{134} - \sigma_3)}$

Molecular volume: $v_{134} = v_{14}\left(1 - \chi_3^{\text{surf}}\right) + v_3\chi_3^{\text{surf}}$

Pseudo-binary solution (134)–surfactant (2) mixture:

Quaternary Eberhart model: $\sigma = f^{EB}\left(x_i^{\text{bulk}}\right)$

Surface composition: $x_2^{\text{surf}} = \dfrac{v_{134}(\sigma_{134} - \sigma)}{v_{134}(\sigma_{134} - \sigma) + v_2(\sigma - \sigma_2)}$

$x_3^{\text{surf}} = \left(1 - x_2^{\text{surf}}\right)\chi_3^{\text{surf}}$

$x_4^{\text{surf}} = \psi_4^{\text{surf}}\left(1 - \chi_3^{\text{surf}}\right)\left(1 - x_2^{\text{surf}}\right)$

$x_1^{\text{surf}} = 1 - x_2^{\text{surf}} - x_3^{\text{surf}} - x_4^{\text{surf}}$

Geometry:

Monolayer thickness: $\delta = \left(\dfrac{6}{\pi}\sum_{i=1}^4 v_i x_i^{\text{surf}}\right)^{1/3}$

Volumes: $V^{\text{bulk}} = \dfrac{\pi}{6}\left(D_{\text{wet}} - 2\delta\right)^3, \ V^{\text{surf}} = V - V^{\text{bulk}}$

Mole numbers: $n_i^{\text{bulk}} = f\left(V^{\text{bulk}}, v_i, x_i^{bulk}\right)$

$n_i^{\text{surf}} = f\left(V^{\text{surf}}, v_i, x_i^{surf}\right)$

Mass closure:
$\epsilon = \sum_{i=1}^4 \left|\dfrac{n_i^{\text{tot}} - n_i^{\text{bulk}} - n_i^{\text{surf}}}{n_i^{\text{tot}}}\right|$

$\epsilon < 10^{-10}$ — False

True

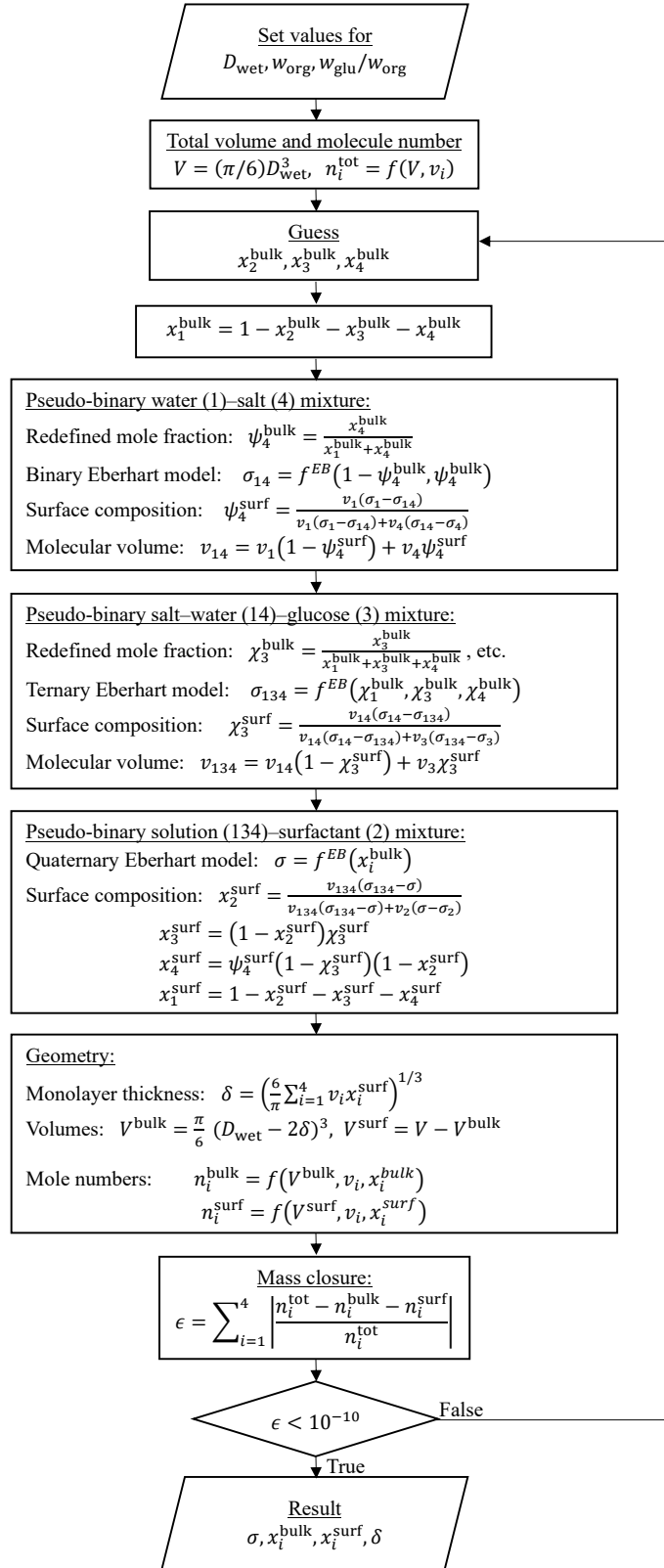Result
$\sigma, x_i^{\text{bulk}}, x_i^{\text{surf}}, \delta$

Figure S2: Flowchart for calculating bulk–surface partitioning with the Eberhart–Monolayer model for a quaternary mixture.

S3 Influence of solution non-ideality

The water activity (Raoult effect) plays an important role in the calculation of the critical supersaturation via Eq. 1. To test the sensitivity of SS_{crit} on the choice of a_w, Köhler curves were constructed based on four different ways to calculate a_w.

First, an ideal solution is assumed, i.e., $a_w = \hat{x}_w$, where $\hat{x}_w$ is calculated based on the dissociation of NaCl into 2 ions and no dissociation of the organic substances (labelled "ideal").

Second, to consider solution non-ideality, a_w is calculated with AIOMFAC. Note that liquid–liquid phase separation is not considered in that calculation, i.e., all substances are forced to be in one phase. We label this second approach "AIOMFAC-1ph".

Third, we calculate a_w assuming that the surfactant is hydrophobic and therefore entirely present in a separate phase, e.g., in the form of micelles or as a surface layer (labelled "surfactant hydrophobic"). In this case, the surfactant is not contributing to the Raoult effect, i.e., the bulk mole fractions are converted to "surfactant-free" mole fractions $\tilde{x}$. For a system of water(1)–surfactant(2)–glucose(3)–NaCl(4), for example, the surfactant-free mole fraction of water would be calculated as $\tilde{x}_1 = x_1/(x_1 + x_3 + x_4)$. Based on $\tilde{x}_1, \tilde{x}_3$, and $\tilde{x}_4$, a_w is calculated with AIOMFAC. We label this third approach as "surfactant hydrophobic".

Fourth, we combine the "surfactant hydrophobic" case with AIOMFAC-1ph by taking the minimum a_w of both.

To test their influence, we use all four assumptions to calculate Köhler curves with either

1. the Eberhart–Monolayer model (a_w is calculated based on x_i^{bulk}, $\sigma = f(x_i^{bulk})$,

2. a calculation neglecting bulk depletion (a_w is calculated based on x_i^{tot}, $\sigma = f(x_i^{tot})$, and

3. Classical Köhler theory (a_w is calculated based on x_i^{tot}, $\sigma = \sigma_1$).

The result of this comparison for an SDS–glucose–NaCl particle of $D_{dry} = 50$ nm particle is shown in Fig. S3. In the second row of all three columns it can be seen that a_w predicted with AIOMFAC-1ph (blue dashed line) is higher than the one assuming a hydrophobic surfactant (yellow dashed line) at low wet diameters. Therefore, the particle is assumed to undergo LLPS in that range and the best estimate (black solid line) follows the "surfactant hydrophobic" calculation. As soon as AIOMFAC-1ph predicts a lower a_w that "surfactant hydrophobic" (blue and yellow lines are crossing), the droplet is assumed to be one homogeneous phase and the best estimate follows AIOMFAC-1ph. This results in a local maximum in a_w, which shows up in the Köhler curve (first row), too. In the first two columns, this local maximum is also the global maximum and marks SS_{crit}. In both the calculation with the Eberhart–Monolayer model and assuming no bulk depletion, during the LLPS the surface tension of the droplet is that of pure SDS ($\sigma = \sigma_2$) leading to a similar Kelvin effect for both assumptions and therefore also to a similar SS_{crit}. The only difference between the two approaches is that in the Eberhart–Monolayer model the bulk is slightly depleted in SDS (see fourth row), which causes the LLPS to stop at a lower wet diameter. In the calculation using classical Köhler theory, $\sigma = \sigma_1$ (see third row) which causes a much higher Kelvin effect and a much higher SS_{crit} than in the first two model approaches.

Figure S4 shows the same calculation for a pinonic acid–NaCl particle of $D_{dry} = 50$ nm and the same trends can be observed as in the previous example. In contrast to the calculation with SDS, here the surface tension is reduced less in the first two columns leading to a smaller difference in SS_{crit} between classical Köhler theory and the first two columns. From these two examples, it can be seen that in cases with high organic fraction and small dry diameters, the particles have little hygroscopic growth and, as a result, are still in a phase-separated state at activation leading to increased SS_{crit} values compared to a calculation assuming ideality.
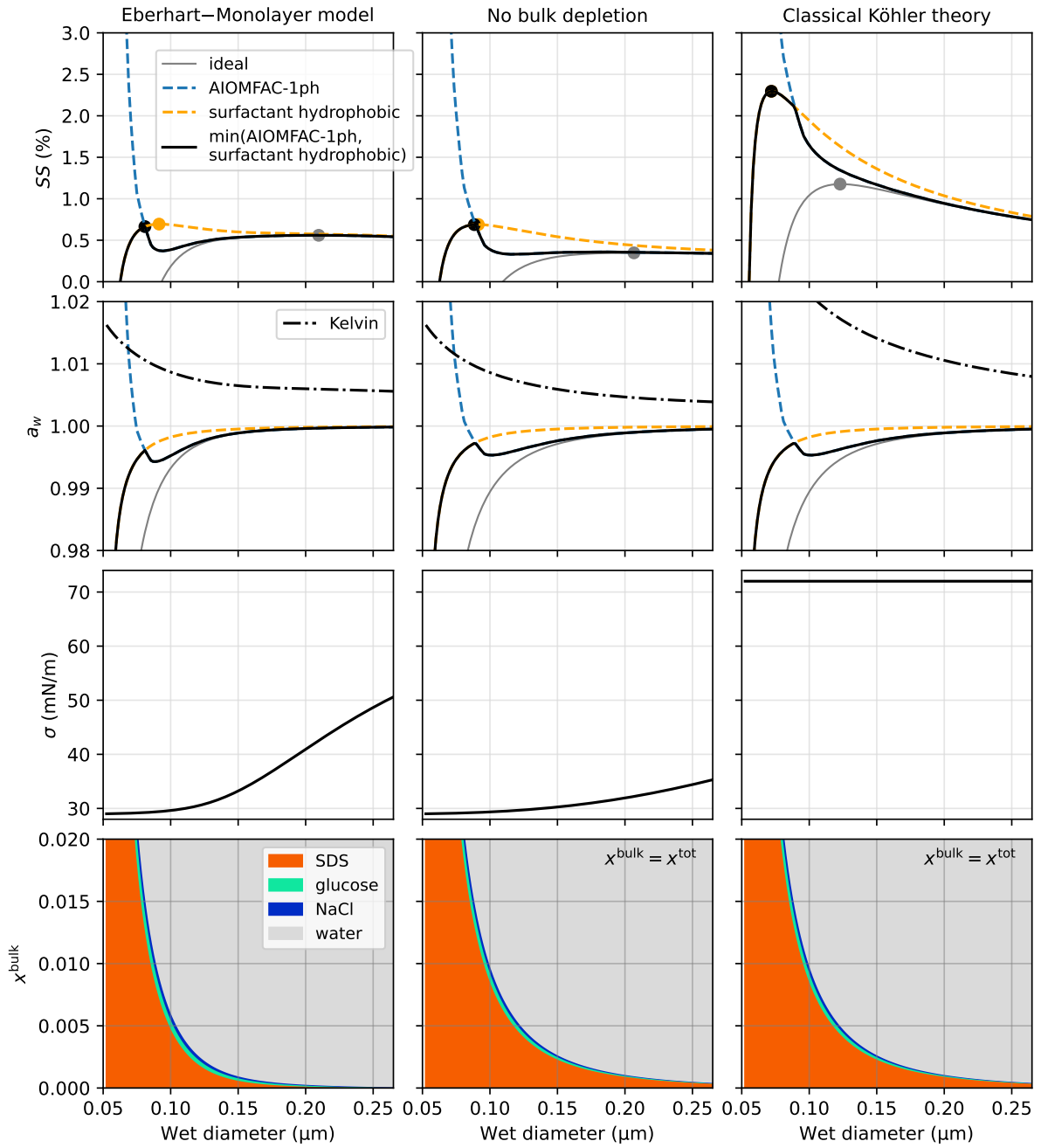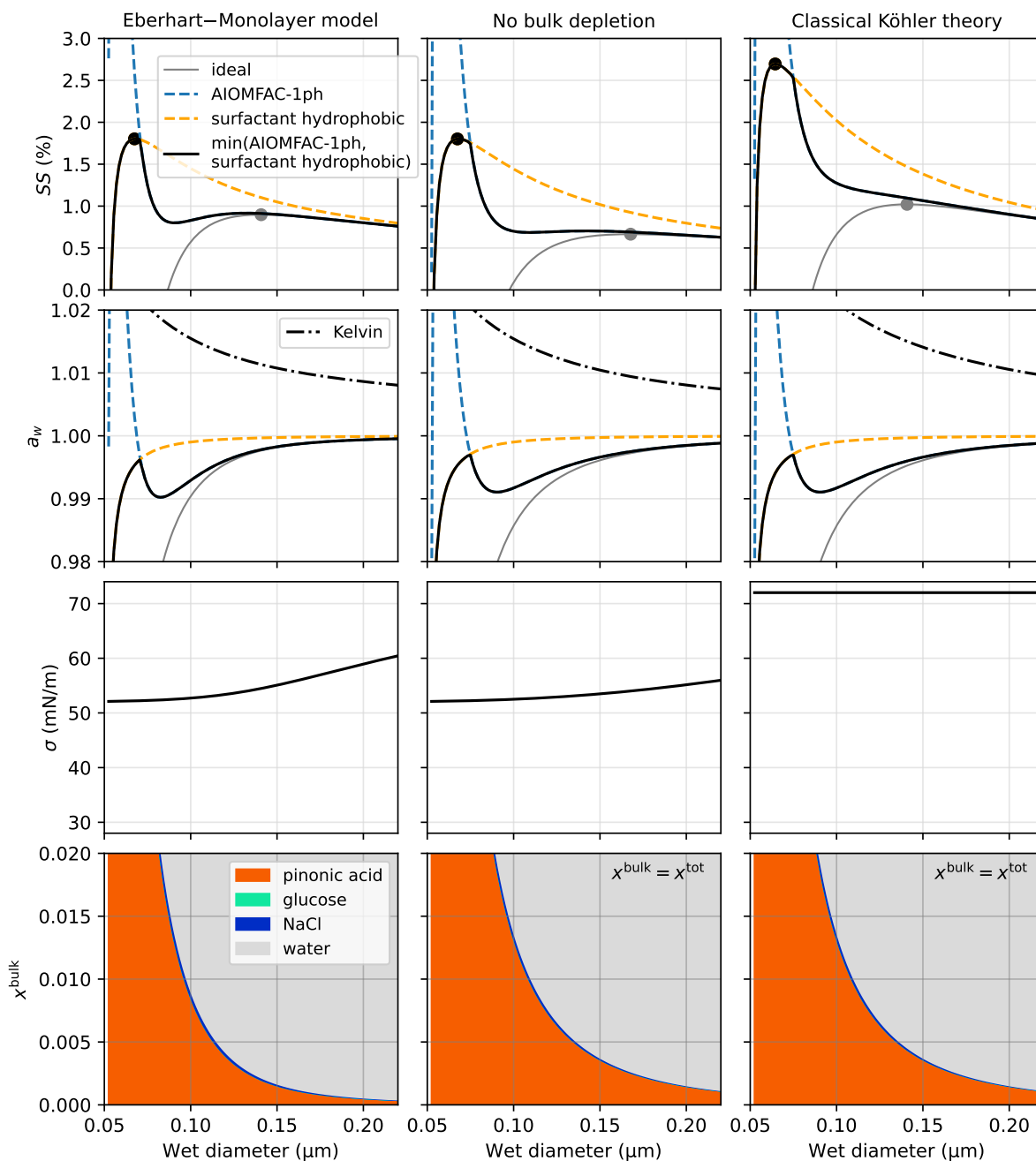
Figure S3: Köhler curves calculated with the Eberhart–Monolayer model, assuming no bulk depletion, and with Classical Köhler theory for a SDS–glucose–NaCl particle with $D_{\mathrm{dry}} = 50\,\mathrm{nm}$, organic fraction "high" and $w_{\mathrm{glu}}/w_{\mathrm{org}} = 0.05$. First row: Köhler curve and critical supersaturation (circle). Second row: water activity a_w (Raoult effect) and saturation ratio of the Kelvin effect, calculated with the exponential function in Eq. 1. Third row: droplet surface tension. Fourth row: bulk composition (first column) and total composition (second and third column). The y-axis range was limited to 0–0.02 for a better visibility of the solute share.

Figure S4: Köhler curves calculated with the Eberhart–Monolayer model, assuming no bulk depletion, and with Classical Köhler theory for a pinonic acid–NaCl particle with $D_{dry} = 50\,\text{nm}$, organic fraction "high" and $w_{glu}/w_{org} = 0$. First row: Köhler curve and critical supersaturation (circle). Second row: water activity a_w (Raoult effect) and saturation ratio of the Kelvin effect, calculated with the exponential function in Eq. 1. Third row: droplet surface tension. Fourth row: bulk composition (first column) and total composition (second and third column). The y-axis range was limited to 0–0.02 for a better visibility of the solute share.

S4 Eberhart fit parameters of organic substances

Table S1: Eberhart fit parameters of acids, alcohols, ketones, and aldehydes shown in Fig. 3. Substances with a star correspond to those denoted by a star in Fig. 3. CI_{95} is the 95 % confidence interval of parameters that were fitted. References for σ_i values from measurements (i.e., that have no CI_{95} value) can be found in El Haber et al. (2024). RMSE is the root mean square error.

No.	name	S_{1i}	$CI_{95}(S_{1i})$	σ_i (mN m^{-1})	$CI_{95}(\sigma_i)$ (mN m^{-1})	σ_1 (mN m^{-1})	RMSE (mN m^{-1})
★	propionic acid	55.3	4.6	26.2		72.0	0.664
★	valeric acid	974.6	36.6	26.7		72.0	0.073
★	glutaric acid	67.3	10.5	53.1	0.8	72.0	0.026
★	pinonic acid	3.7e3	1.5e3	52.1	3.6	72.0	0.075
★	oleic acid	9.9e6	4.4e6	32.2		72.0	0.618
1	formic acid	5.4	0.5	37.5		72.0	0.014
2	acetic acid	15.6	1.3	27.9		72.0	0.257
3	butyric acid	199.2	12.1	26.2		72.0	0.053
4	oxalic acid	16.8	9.4	62.7	3.4	72.0	0.117
5	methanesulfonic acid	13.9	2.4	53.0		72.0	0.002
6	malonic acid	26.7	5.8	60.5	0.9	72.0	0.068
7	maleic acid	33.4	8.6	55.2	1.5	72.0	0.062
8	caproic acid	4.5e3	4.5e2	27.5		72.0	0.037
9	succinic acid	119.1	55.1	64.2	1.8	72.0	0.024
10	malic acid	35.2	15.7	66.2	0.9	72.0	0.021
11	caprylic acid	4.2e4	7.8e3	28.8		72.0	0.714
12	adipic acid	596.2	228.0	60.8	2.3	72.0	0.09
13	pelargonic acid	2.0e5	2.2e4	27.9		72.0	0.412
14	citric acid	87.8	48.7	65.1	1.0	72.0	0.067
15	ricinoleic acid	1.9e6	4.8e5	32.9	1.7	72.0	0.421
16	arachidonic acid	5.2e6	1.5e6	29.0	2.6	72.0	0.003
17	methanol	7.3	0.3	23.5		72.0	0.016
18	ethanol	20.1	0.8	22.2		72.0	0.458
19	acetone	24.7	2.4	23.5		72.0	0.385
20	propan-1-ol	95.0	7.0	24.0		72.0	0.394
21	propan-2-ol	69.8	7.6	23.5		72.0	0.734
22	ethylene glycol	6.6	0.5	46.6		72.0	0.038
23	propylene glycol	14.8	0.8	35.9		72.0	0.07
24	propane-1,3-diol	12.8	2.2	46.3		72.0	0.216
25	pentan-1-ol	1.3e3	1.4e2	25.2		72.0	0.105
26	1,3-butanediol	27.2	3.1	37.0		72.0	0.291
27	1,4-butanediol	22.9	3.6	43.8		72.0	0.275
28	glycerol	4.4	0.9	63.0		72.0	0.031
29	hexan-1-ol	4.3e3	4.5e2	25.8		72.0	0.028
30	hexan-2-ol	2.6e3	1.1e2	24.5		72.0	0.374
31	2,3-dimethylbutan-2-ol	1.2e3	9.7e1	23.7		72.0	0.753
32	2-methylpentan-2-ol	1.8e3	1.1e2	23.7		72.0	0.317
33	1,5-pentanediol	355.2	175.9	44.2		72.0	0.22
34	heptan-1-ol	2.3e4	3.9e3	26.6		72.0	0.108
35	hexane-1,2-diol	707.7	69.7	23.8		72.0	0.364
36	hexane-1,6-diol	324.1	38.0	42.3	0.7	72.0	0.061
37	hexane-1,5-diol	234.3	31.5	33.9		72.0	0.042
38	hexane-2,5-diol	132.0	20.1	31.6		72.0	0.522
39	octan-1-ol	3.6e4	8.8e3	27.2		72.0	0.144
40	2,3-dihydroxynaphthalene	5.2e4	8.3e3	48.2	1.0	72.0	0.006

Table S1 (continued): Eberhart fit parameters of sugars, amines, surfactants, and macromolecules shown in Fig. 3. Substances with a star correspond to those denoted by a star in Fig. 3. CI_{95} is the 95 % confidence interval of parameters that were fitted. References for σ_i values that have been measured (i.e., that have no CI_{95} value) can be found in El Haber et al. (2024). RMSE is the root mean square error.

No.	name	S_{1i}	$CI_{95}(S_{1i})$	σ_i (mN m^{-1})	$CI_{95}(\sigma_i)$ (mN m^{-1})	σ_1 (mN m^{-1})	RMSE (mN m^{-1})
41	colamine	6.8	1.2	48.4		72.0	0.258
42	pyrrolidine	25.3	6.9	29.7		72.0	1.223
43	threamine	9.8	2.5	37.4		72.0	0.351
44	3-aminopropan-1-ol	6.5	0.5	44.3		72.0	0.046
45	2-(methylamino)ethan-1-ol	9.6	1.3	35.3		72.0	0.208
46	piperidine	108.1	37.0	29.5		72.0	1.051
47	2-(ethylamino)ethan-1-ol	26.6	8.5	32.2		72.0	1.108
48	cyclohexanamine	885.3	140.5	32.1		72.0	0.741
49	diolamine	9.8	2.3	47.2		72.0	0.035
50	methyl diethanolamine	19.3	2.4	38.2		72.0	0.164
51	DL-norleucine	568.3	561.2	68.1	2.4	72.0	0.016
52	hexamethylenetetramine	117.8	6.8	62.3	0.1	72.0	0.006
53	trolamine	23.1	0.2	46.0		72.0	0.015
54	levoglucosan	45.3	94.0	69.5	2.0	72.0	0.508
55	D-(+)-maltose	9.0	6.7	63.9	4.8	72.0	0.009
★	SDS	1.4e4	2.7e3	29.0	2.6	72.0	0.591
56	DTAB	8.3e3	2.1e3	28.6	3.6	72.0	0.579
57	CTAB	1.5e5	1.9e4	29.2	1.8	72.0	0.259
58	AOT	1.3e5	2.1e4	27.6	1.4	72.0	0.301
59	Triton X114	5.5e6	1.6e6	30.2	1.4	72.0	0.528
60	Brij35	5.5e6	1.4e6	43.7	1.2	72.0	0.165
61	mono-rhamnolipid	7.7e6	2.7e6	27.0	2.9	72.0	0.858
62	di-rhamnolipid	7.0e6	1.8e6	30.4	2.1	72.0	0.434
63	surfactin	1.4e7	7.7e6	27.9	5.6	72.0	0.191
64	syringafactin B/C	4.3e5	1.8e5	19.7	6.2	72.0	0.609
65	viscosin	8.4e6	4.2e6	23.9	5.8	72.0	0.359
66	Suwannee river fulvic acid	1.3e4	3.7e3	39.9	2.7	72.0	0.276
67	NAFA	8.5e4	3.3e4	45.1	5.0	72.0	0.156
68	Humic acid	1.7e4	1.4e4	54.0	3.9	72.0	0.045
69	HULIS	1.9e5	1.6e5	45.5	5.9	72.0	0.229
70	Macromolecules EPS	5.4e7	3.1e7	56.0	2.6	72.0	0.209

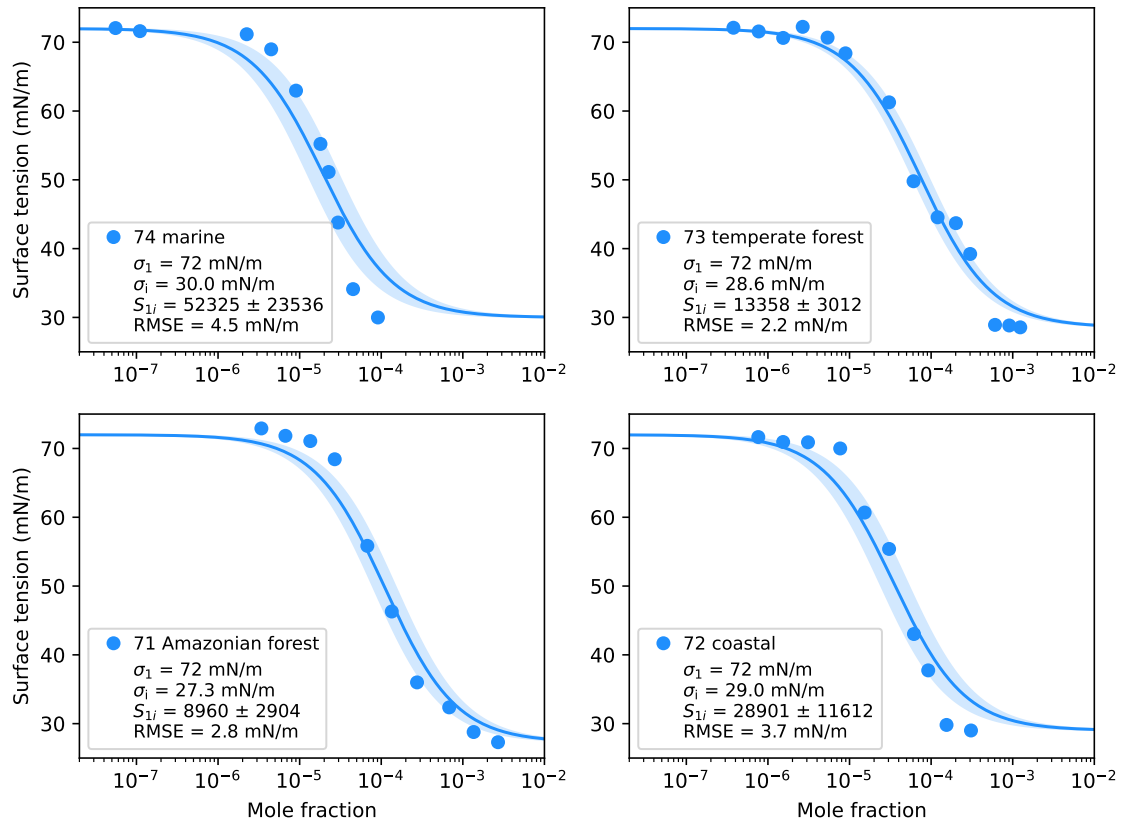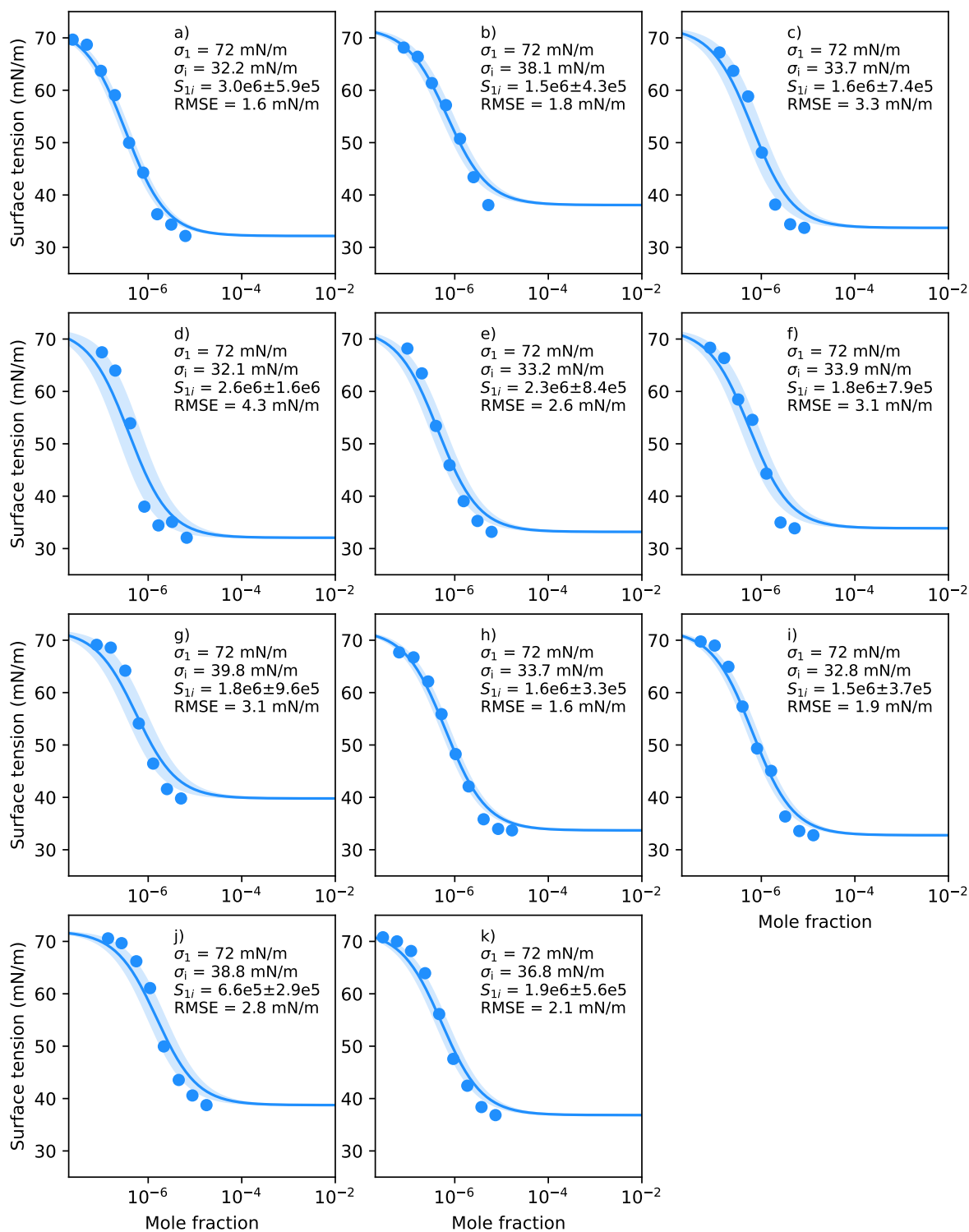# S5 Surface tension isotherms of atmospheric samples

Figure S5: Eberhart model (Eq. 3) fits (solid lines) to surface tension data (markers) of atmospheric sample extracts from Ekström et al. (2010) taken at four different locations. Numbers 71–74 refer to the numbering in Fig. 3. Colored shading shows the 95 % confidence interval. In the legend, the model parameters are given. σ_1 was set to $72\,\text{mN}\,\text{m}^{-1}$ for all samples and σ_i was taken to be the minimum of the experimental data. S_{1i} was fitted and its 95 % confidence interval is given as the uncertainty. RMSE is the root mean square error.

Figure S6: Eberhart model (Eq. 3) fits (solid lines) to surface tension data (markers) of 11 atmospheric sample extracts (a–k) from Gérard et al. (2016) taken at the Baltic Coast at Askö in Sweden. Colored shading shows the 95 % confidence interval. In each panel, the model parameters are shown. σ_1 was set to $72\,\mathrm{mN\,m^{-1}}$ for all samples and σ_i was taken to be the minimum of the experimental data. S_{1i} was fitted and its 95 % confidence interval is given as the uncertainty. RMSE is the root mean square error.

10

S6 Surface tension isotherms of the model compounds
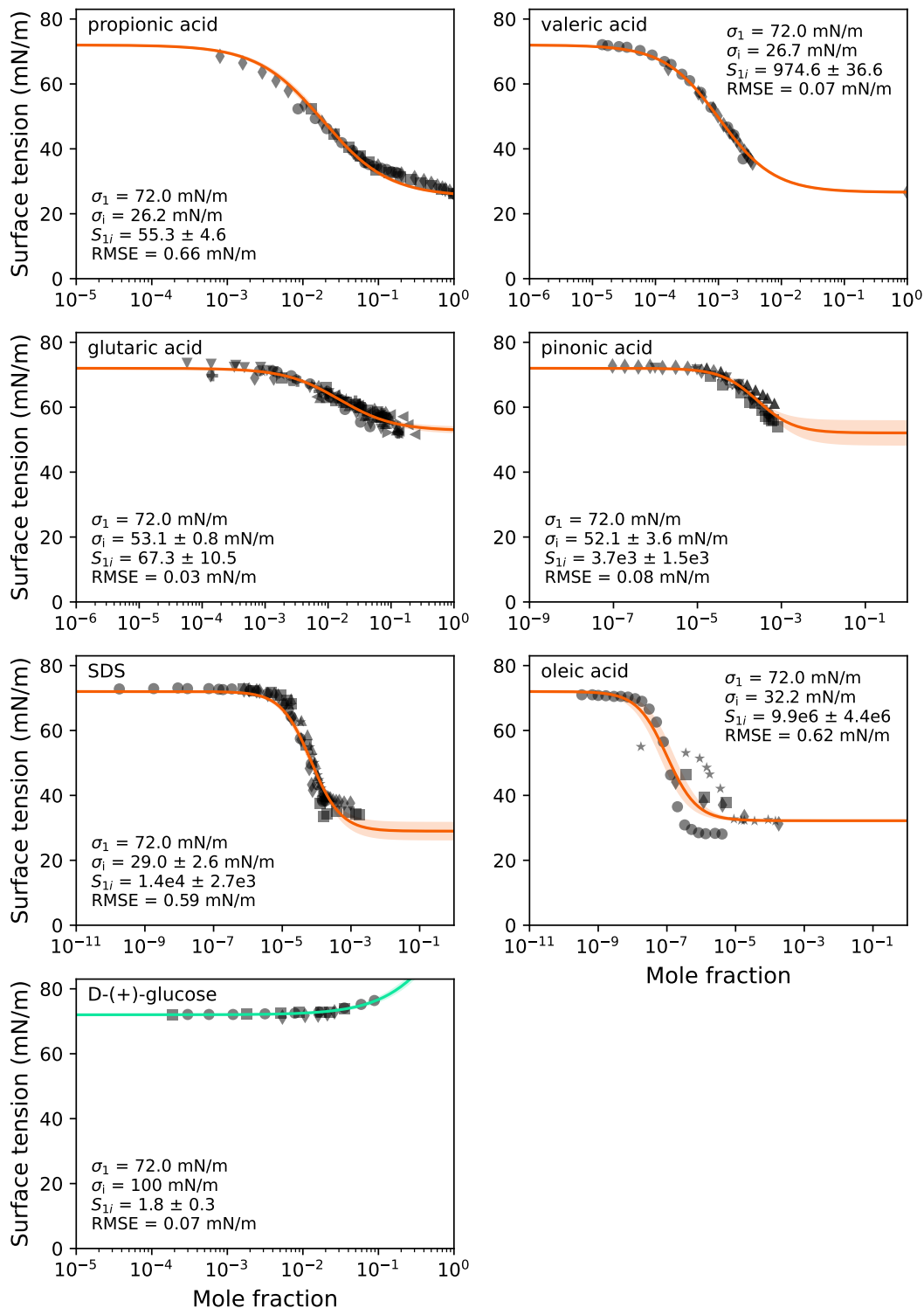
Figure S7: Binary surface tension data (black markers) and Eberhart model fits (colored solid lines) for the model compounds in this study. Fit parameters are annotated in the respective panel together with the root mean square error (RMSE). The colored shading represents the 95 % confidence interval of the fit. Different markers represent different datasets. For reference of the underlying data refer to El Haber et al. (2024). For NaCl, refer to Kleinheins et al. (2023).

S7 Influence of salting-out
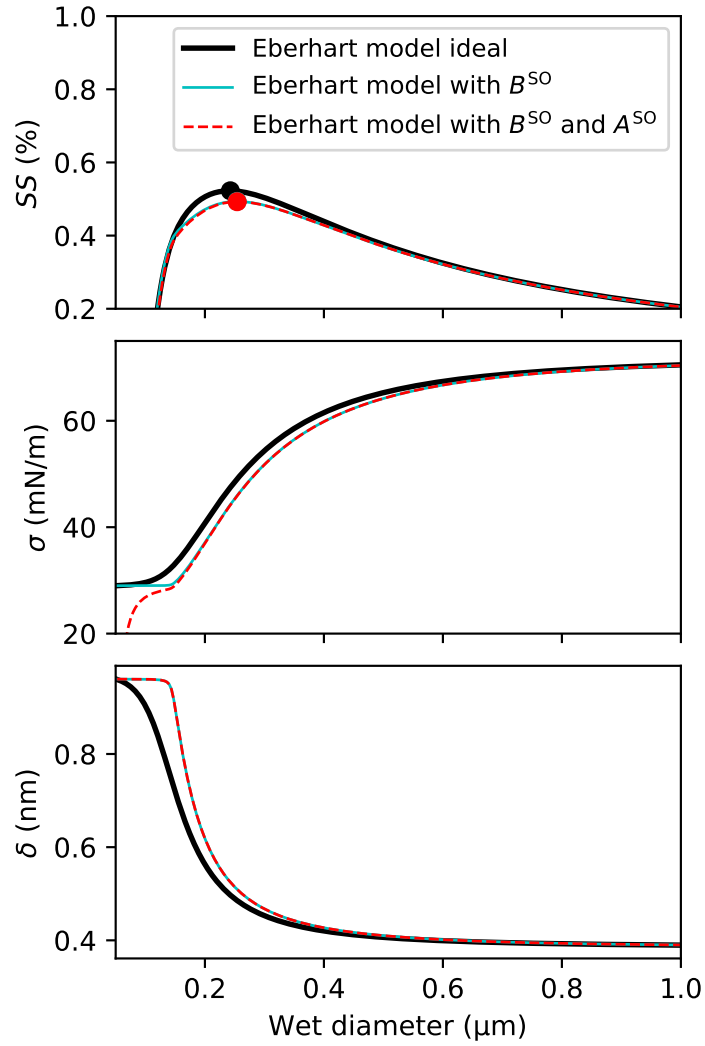
Figure S8: Influence of surface tension non-ideality (salting-out) on the supersaturation SS, droplet surface tension σ, and the monolayer thickness δ, using an artificially high salting-out factor of $B_{24}^{\mathrm{SO}} = 10^5$. Three cases are distinguished: assuming ideality (solid black lines, $A_{24}^{\mathrm{SO}} = 0$, $B_{24}^{\mathrm{SO}} = 0$), considering bulk related salting-out (solid cyan lines $A_{24}^{\mathrm{SO}} = 0$, $B_{24}^{\mathrm{SO}} = 10^5$), and considering bulk and surface related salting-out (dashed red line, $A_{24}^{\mathrm{SO}} = 22.63$, $B_{24}^{\mathrm{SO}} = 10^5$). In all cases, $D_{\mathrm{dry}} = 50\,\mathrm{nm}$, $w_{\mathrm{org}} = 0.93$ ("med"), and $w_{\mathrm{glu}}/w_{\mathrm{org}} = 0$. First row: Köhler curve and critical supersaturation (circle), second row: droplet surface tension, third row: surface monolayer thickness.

S8 Köhler curves of additional systems
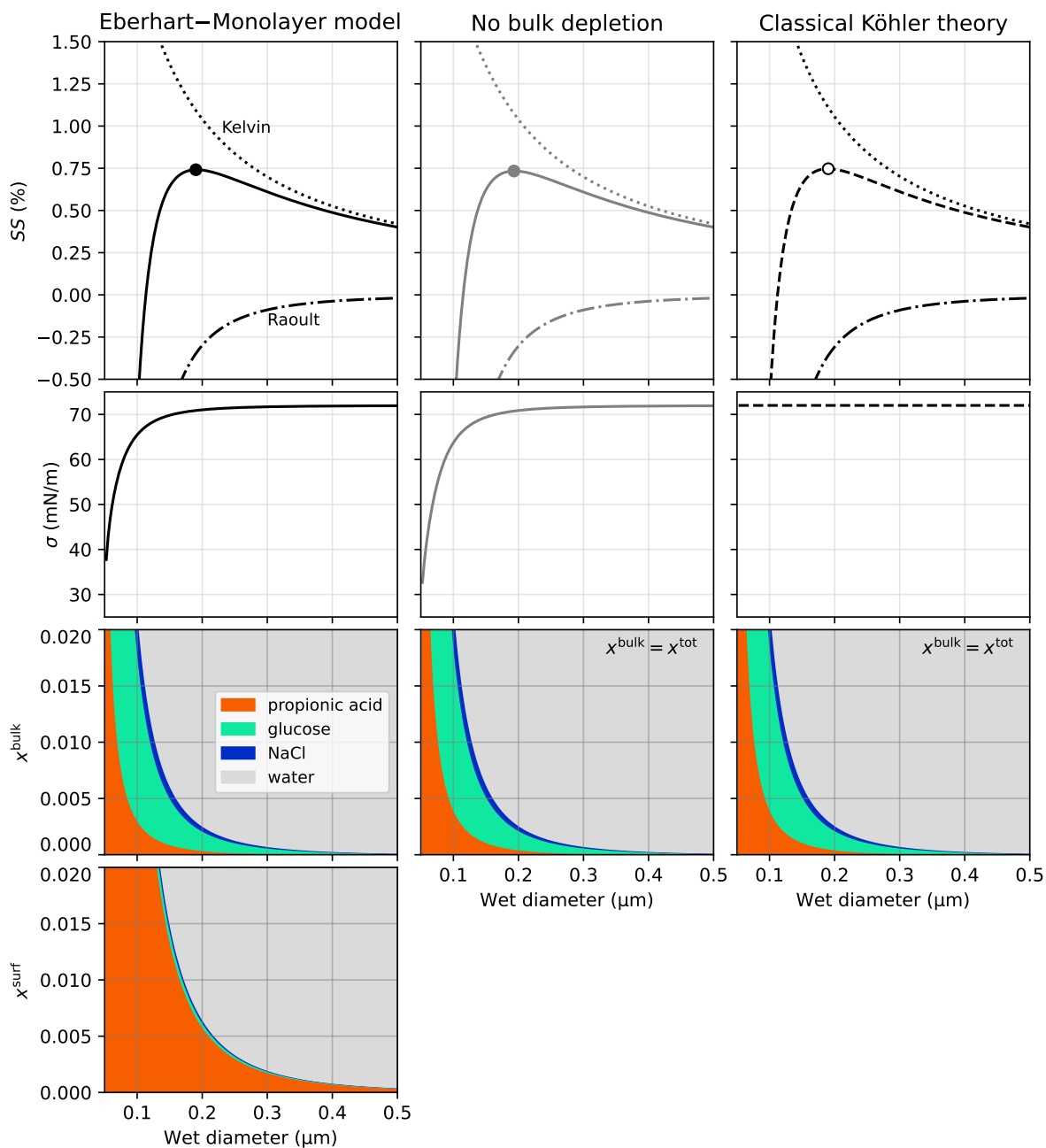
Figure S9: Same as Fig. 4 but using propionic acid instead of SDS and a high fraction of glucose ($w_{\mathrm{glu}}/w_{\mathrm{org}} = 0.9$). In the third and fourth row, the y-axis range was limited to 0–0.02 for a better visibility of the solute share.
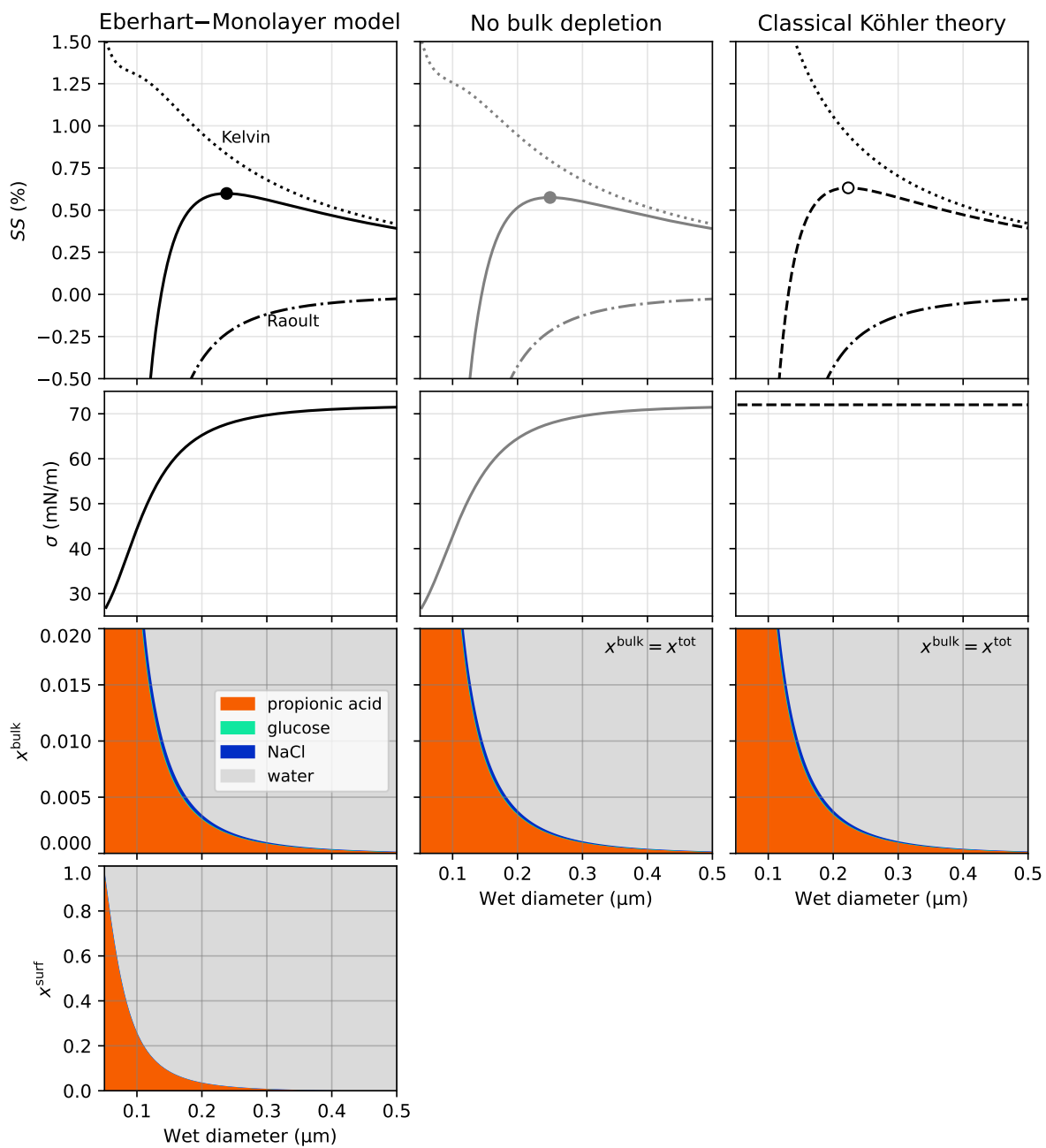
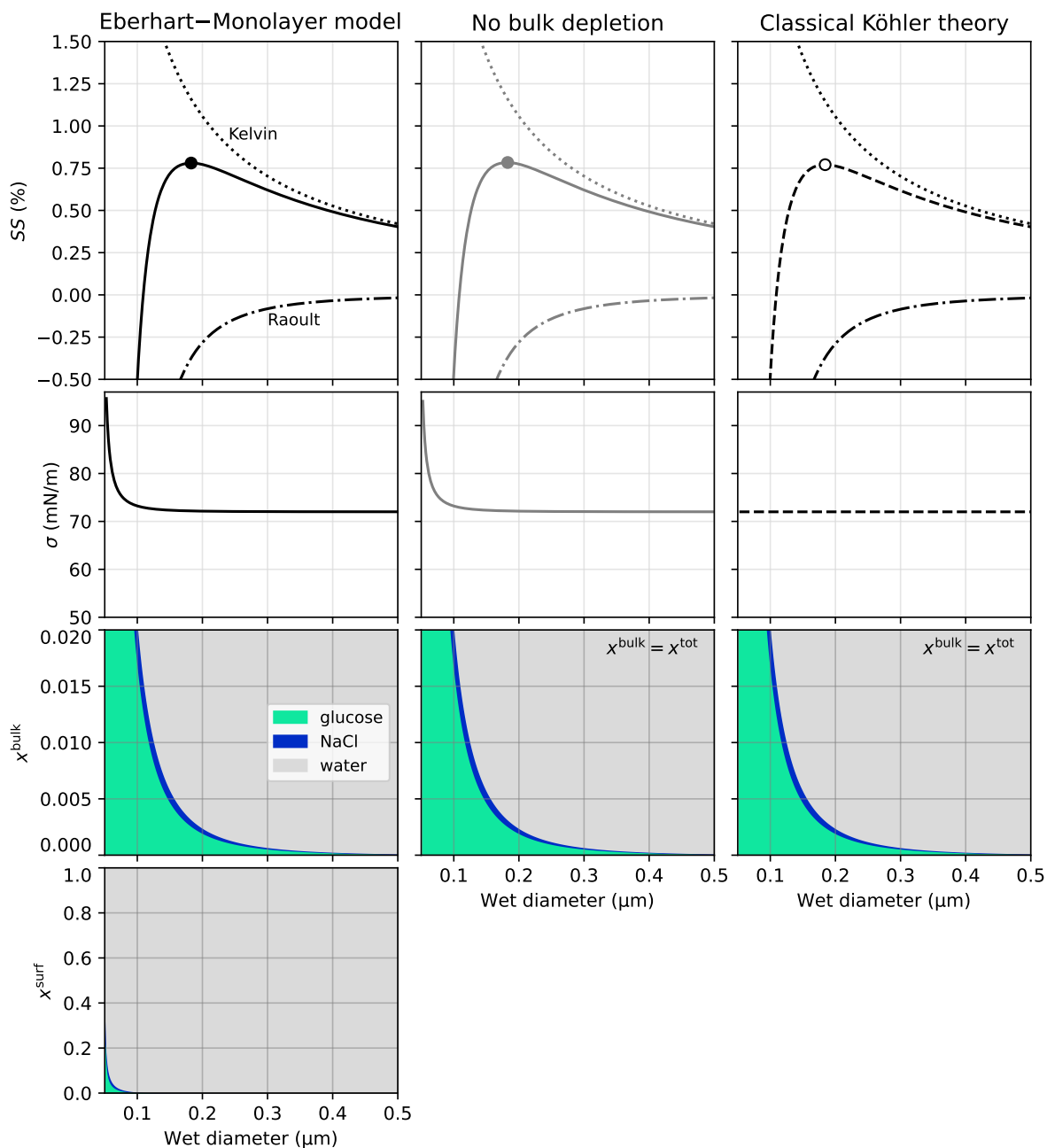Figure S10: Same as Fig. 4 but using propionic acid instead of SDS.

Figure S11: Köhler curves calculated with the Eberhart–Monolayer model, assuming no bulk depletion, and with Classical Köhler theory for a ternary glucose–NaCl–water particle (i.e., $w_{glu}/w_{org} = 1$) with $D_{dry} = 50\,\text{nm}$ and $w_{org} = 0.93$ (”med”). First row: Köhler curve (solid or dashed line) with Raoult (dash-dotted lines) and Kelvin effect (dotted lines) and critical supersaturation (circle). Second row: droplet surface tension. Third row: bulk composition (first column) and total composition (second and third column). The y-axis range was limited to 0–0.02 for a better visibility of the solute share. Fourth row: surface composition in the Eberhart–Monolayer model. For consistency with the previous plots, the y-axis range is kept here at 0–1. Since no partitioning is calculated in the second and third column, the surface composition is not determined and hence not shown here.
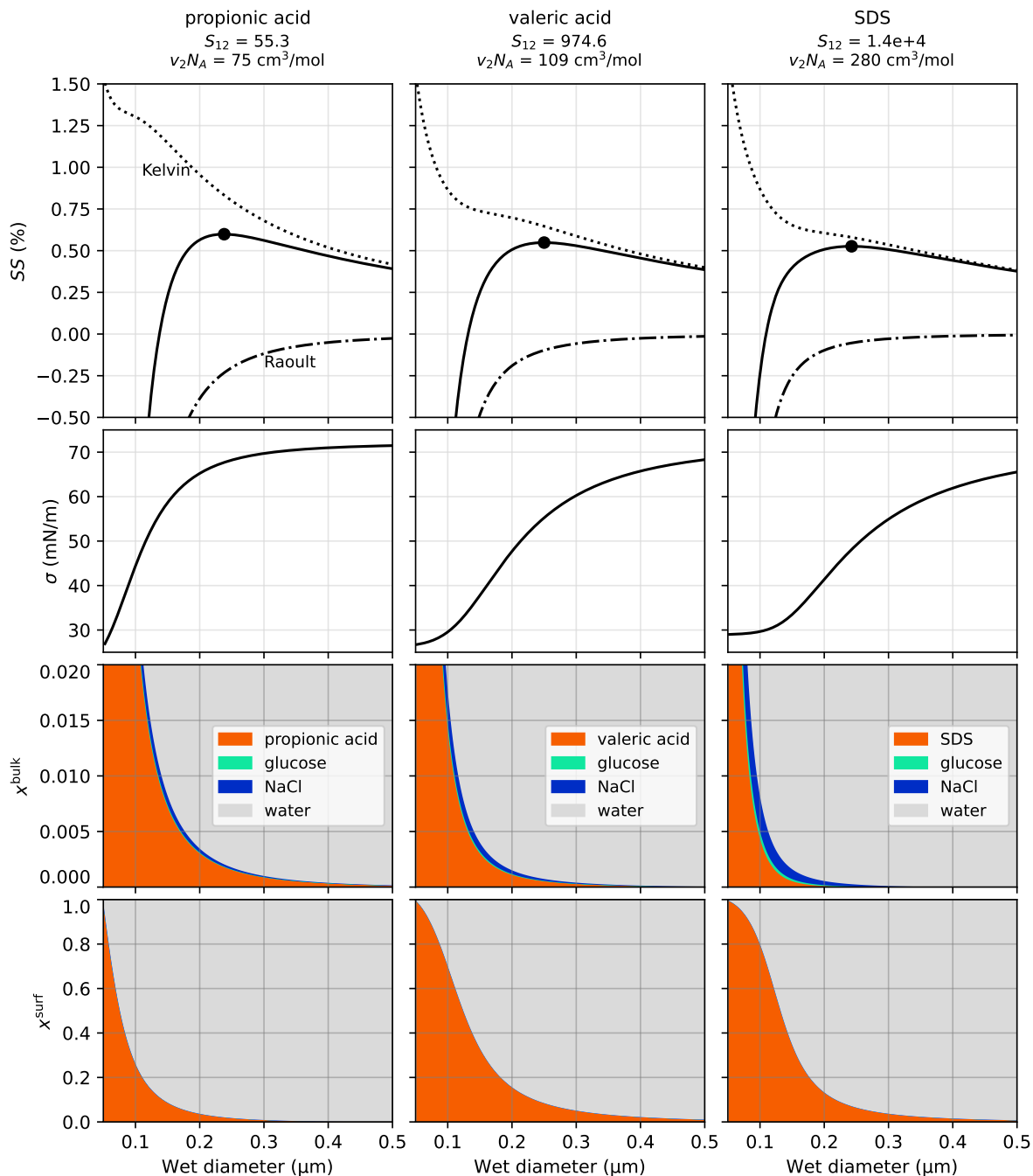
S9   Variation of the surfactant

Figure S12: Köhler curves to illustrate the effect of molar volume v_2N_A on the Raoult effect and separation factor S_{12} on the Kelvin effect calculated with the Eberhart–Monolayer model for three different surfactants in a quaternary surfactant–glucose–NaCl–water particle ($D_{\mathrm{dry}} = 50\,\mathrm{nm}$, $w_{\mathrm{org}} = 0.93$ ("med"), and $w_{\mathrm{glu}}/w_{\mathrm{org}} = 0.05$). First row: Köhler curve (solid or dashed line) with Raoult (dash-dotted lines) and Kelvin effect (dotted lines) and critical supersaturation (circle), second row: droplet surface tension, third row: bulk composition, and fourth row: surface composition. The y-axis range in the third row was limited to 0–0.02 for a better visibility of the solute share.
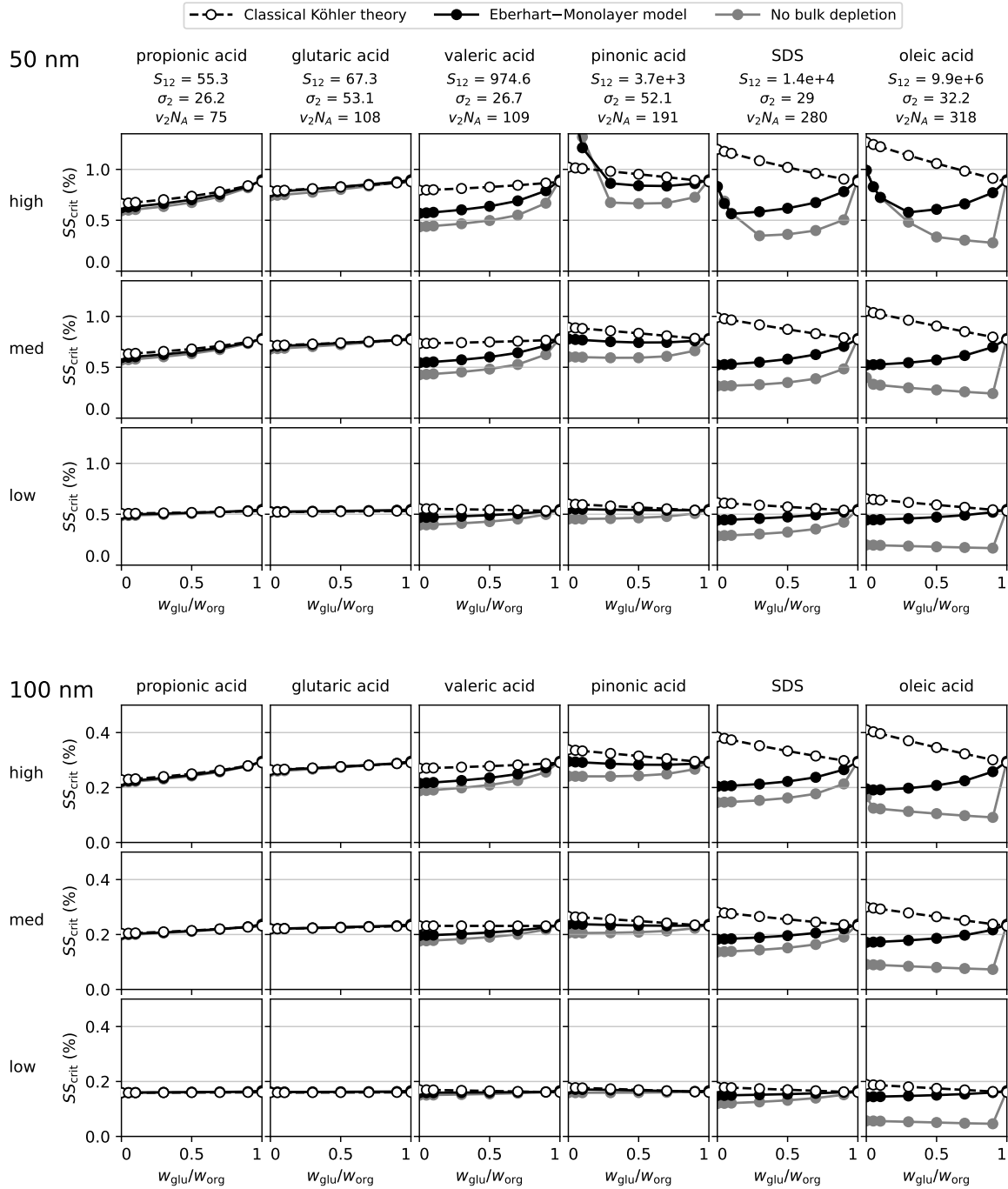
Figure S13: Combined influence of surfactant properties and the organic fraction on critical supersaturation for two different particle sizes. Upper panel: $D_{\mathrm{dry}} = 50\,\mathrm{nm}$. Lower panel: $D_{\mathrm{dry}} = 100\,\mathrm{nm}$. In the column title, the name of the surfactant, its binary separation factor in water S_{12}, its pure component surface tension in $\mathrm{mN\,m^{-1}}$, and its molar volume in $\mathrm{cm^3\,mol^{-1}}$ is given. The organic fraction w_{org} for each row can be found in Table 1. In some of the calculations with glutaric acid and propionic acid all curves overlap.

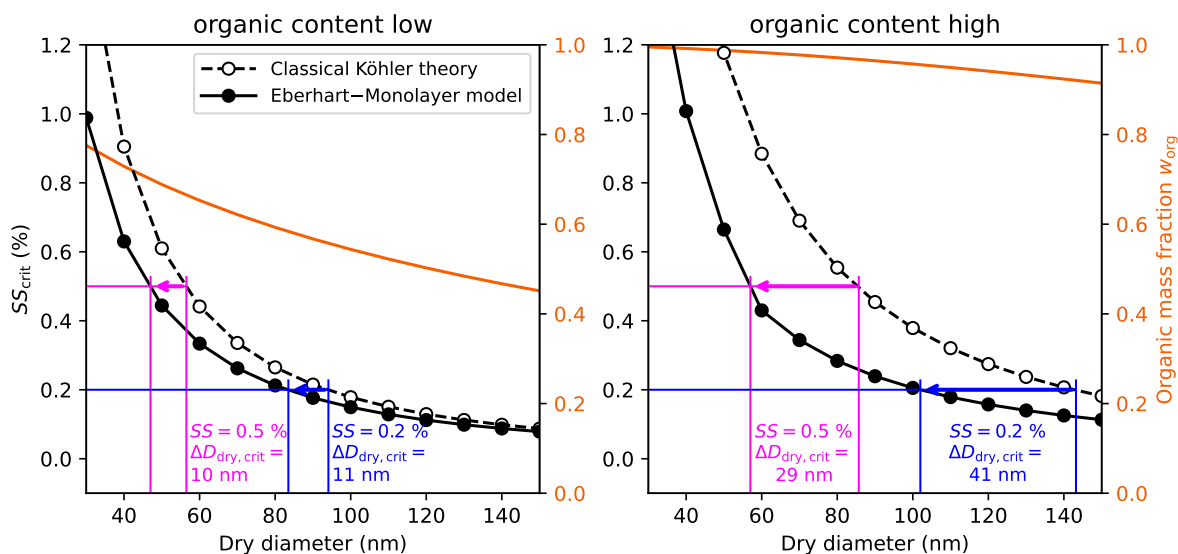# S10 Influence of organic fraction on the critical activation diameter

Figure S14: Same as Fig. 8 but with low organic content (left panel) and high organic content (right panel). The organic fraction is shown with an orange solid line on the right y-axis.

References

Ekström, S., Nozière, B., Hultberg, M., Alsberg, T., Magnér, J., Nilsson, E. D., and Artaxo, P.: A possible role of ground-based microorganisms on cloud formation in the atmosphere, Biogeosciences, 7, 387–394, https://doi.org/10.5194/bg-7-387-2010, 2010.

El Haber, M., Gérard, V., Kleinheins, J., Ferronato, C., and Nozière, B.: Measuring the Surface Tension of Atmospheric Particles and Relevant Mixtures to Better Understand Key Atmospheric Processes, Chem. Rev., https://doi.org/10.1021/acs.chemrev.4c00173, 2024.

Gérard, V., Nozière, B., Baduel, C., Fine, L., Frossard, A. A., and Cohen, R. C.: Anionic, Cationic, and Nonionic Surfactants in Atmospheric Aerosols from the Baltic Coast at Askö, Sweden: Implications for Cloud Droplet Activation, Environmental Science & Technology, 50, 2974–2982, https://doi.org/10.1021/acs.est.5b05809, pMID: 26895279, 2016.

Kleinheins, J., Shardt, N., El Haber, M., Ferronato, C., Nozière, B., Peter, T., and Marcolli, C.: Surface tension models for binary aqueous solutions: a review and intercomparison, Phys. Chem. Chem. Phys., 25, 11 055–11 074, https://doi.org/10.1039/D3CP00322A, 2023.